SLAC-PUB-15635

Constraining Dark Matter in Galactic Substructure

Eric J. Baxter[1], Scott Dodelson[1,2,3], Savvas M. Koushiappas[4], Louis E. Strigari[5]
[1]*Department of Astronomy & Astrophysics, The University of Chicago, Chicago, IL 60637*
[2]*Center for Particle Astrophysics, Fermi National Accelerator Laboratory, Batavia, IL 60510*
[3]*Kavli Institute for Cosmological Physics, Chicago, IL 60637*
[4]*Department of Physics, Brown University, Providence, RI 02912 and*
[5]*Kavli Institute for Particle Astrophysics and Cosmology, Stanford University, Stanford, CA 94305*
(Dated: September 13, 2010)

Detecting the dark matter annihilation signal from Galactic substructure, or subhalos, is an important challenge for high-energy gamma-ray experiments. In this paper we discuss detection prospects by combining two different aspects of the gamma-ray signal: the angular distribution and the photon counts probability distribution function (PDF). The true PDF from subhalos has been shown recently (by Lee et al.) to deviate from Poisson; we extend this analysis and derive the signal PDF from a detailed ΛCDM-based model for the properties of subhalos. We combine our PDF with a model for Galactic and extra-Galactic diffuse gamma-ray emission to obtain an estimator and projected error on dark matter particle properties (mass and annihilation cross section) using the Fermi Gamma-Ray Space Telescope. We compare the estimator obtained from the true PDF to that obtained from the simpler Poisson analysis. We find that, although both estimators are unbaised in the presence of backgrounds, the error on dark matter properties derived from the true PDF is $\sim 50\%$ smaller than when utilizing the Poisson-based analysis.

PACS numbers: 95.35.+d; 95.85.Pw

I. INTRODUCTION

A wide variety of evidence points to the existence of nonbaryonic dark matter [1]. There are three ways of directly confirming this hypothesis: producing dark matter or its cousins in an accelerator [2, 3], directly detecting dark matter particles impinging on the Earth in underground detectors [4, 5], and indirectly detecting dark matter by observing the products of an annihilation of two dark matter particles in space [6–8]. The current excitement in the field stems from the coincidental maturity of all three of these techniques. The Large Hadron Collider began operations in 2009, a number of direct detection experiments have proven their ability to scale up to the one-ton level, and there are several experiments (Fermi Gamma-Ray Satellite Telescope [9], Atmospheric Cerenkov Telescopes [10], PAMELA [11], Ice Cube [12]) poised to detect the indirect signal.

For gamma-ray experiments a key challenge is to extract the dark matter signal in the presence of emission from point sources, such as pulsars and AGN, and diffuse sources such as cosmic rays. One way to discriminate photons produced by a given dark matter source from the above backgrounds is to measure the energy spectrum. Photons generated by the annihilation of standard thermally-produced particle dark matter have a spectrum characteristic of quark production and hadronization[13, 14], distinguishing them from the typical power law-like behavior of other sources [15, 16]. A second discriminant is the angular distribution [17–21]. The angular distribution of photons produced in dark matter annihilations results from the variation of the dark matter density profile as a function of ψ, the angle between the incoming direction and the line connecting us to the Galactic center. By contrast, the extra-Galactic background [22, 23] is more or less isotropic, and the diffuse Galactic background is predominantly confined to the Galactic disk.

Recently, several groups [24–26] have explored the possibility of indirect detection in the Milky Way halo by adding another discriminant, the probability distribution function (PDF). In their recent analysis Lee et al. [24] have determined the PDF of photons produced by dark matter annihilations in dark matter substructure (subhalos) in our Galaxy, and they have shown that this PDF is clearly distinct from a Poisson distribution. In particular, for a given pixel observed by, e.g., the Fermi telescope, there is an unusually large probability (unusual compared with Poisson expectation for the same mean number of counts) of observing multiple counts from the population of subhalos along the line-of-sight.

Here we test the idea of using the PDF, together with a ΛCDM-based model for the scatter in subhalo properties, to extract the dark matter signal in the Fermi experiment. In this work we are in particular interested in answering the following questions:

- Can the PDF – if known – be used as an effective tool to extract the dark matter signal?
- Will Fermi have the statistical reach to probe a velocity-weighted annihilation cross section of 3×10^{-26} cm^3 sec^{-1}, the canonical value for a thermally produced dark matter candidate?

Published in Phys.Rev.D82:123511,2010 and arXiv:1006.2399.

Work supported in part by US Department of Energy under contract DE-AC02-76SF00515.

SLAC National Accelerator Laboratory, Menlo Park, CA 94025

- Does one need to know the PDF in order to analyze an experiment? I.e., if one incorrectly assumes a χ^2 distribution, will s/he be led to incorrect conclusions about the parameters under consideration?

For concreteness, throughout, we make predictions and projections for one year of Fermi data.

The layout of this paper is as follows. §II describes the 3-component model of subhalo, diffuse Galactic and extra-Galactic emission that we use. Simulated maps of these components are produced in §III. We then analyze the maps two different ways in §IV: with a standard χ^2 analysis and with the exact likelihood. The former does not use the information contained in the PDF, while the latter analysis does use this information. Our conclusions are presented in §V.

II. THE MODEL

We assume a three-component model for the diffuse gamma-ray background: annihilation radiation from dark matter subhalos, Galactic emission, and extra-Galactic emission. This simplified model neglects other contributions to the gamma-ray background, including point sources – both Galactic and extra-Galactic – which we assume can be identified and removed. We also neglect other dark matter sources, including diffuse emission from the Milky Way halo and from cosmological halos, as we are in particular concerned with isolating the subhalo contribution. Given the latitudes that we consider for our analysis this model is appropriate [27]. As we argue here, even our simplified model represents an improvement in our understanding of diffuse emission from subhalos and our ability to extract it using gamma-ray data. In the context of the larger goal of detecting dark matter our assumptions may be viewed as conservative, as we are neglecting several possible sources of signal.

Following Lee et al. [24], we write the probability of obtaining C_i counts in bin i which is an angle ψ_i away from the Galactic center as

$$P(C_i) = \int dF P_{sh}(F;\psi_i)\mathcal{P}[E_i F + C_i^{\rm gal} + C_i^{\rm eg}; C_i], \tag{1}$$

where $P_{sh}(F;\psi_i)$ is the probability of subhalos producing a flux F which depends on ψ_i in the pixel; $\mathcal{P}$ is the Poisson probability for obtaining C_i counts if the mean number of counts is equal to F multiplied by the exposure of the pixel in the experiment, E_i, plus the counts expected from the two background sources, $C_i^{\rm gal}$ and $C_i^{\rm eg}$. We are implicitly assuming here that the PDF's of both background components – Galactic and extra-Galactic – are Poisson, as opposed to the PDF of the subhalo contribution which is captured in P_{sh}. This is the best one could hope for when examining the utility of the PDF; if the PDF turns out not to matter much in our analysis, then this will be a robust conclusion. In the rest of this section, we describe the details of this model, now specified by $P_{sh}(F;\psi_i)$ and the expected number of counts due to backgrounds $C_i^{\rm gal}$ and $C_i^{\rm eg}$.

A. The Signal: Emission from Subhalos

In order to calculate the counts probability distribution function given in Eq. 1, we must estimate the flux probability distribution $P_{sh}(F;\psi_i)$, which depends on a description of the abundance and properties of all subhalos along the line of sight. Following Lee et al. [24], we first calculate $P_1(F;\psi_i)$, the probability of observing a flux F from a *single* subhalo at angle ψ_i from the Galactic center:

$$P_1(F;\psi_i) \propto \Theta(F_{\rm max} - F)\int_0^{\ell_{\rm max}} d\ell \int dL_{sh}\, P(L_{sh},\ell,\psi_i)\delta\left(F - \frac{L_{sh}}{4\pi\ell^2}\right). \tag{2}$$

Here, $P(L_{sh},\ell,\psi_i)$ is the probability of finding a subhalo emitting luminosity L_{sh} at a distance ℓ from us at an angle ψ_i from the Galactic center. The step function limits the flux to be less than $F_{\rm max}$ since sources with larger fluxes will be identified as resolved point sources. Although the resolved flux limit of Fermi depends on energy[1], for concreteness we choose a simple threshold of $F_{\rm max} = 10^{-9}{\rm cm}^{-2}{\rm s}^{-1}$. The line-of-sight integral extends out to $\ell_{\rm max}$, which is determined by the assumed extent of the dark matter halo. The probability $P(L_{sh},\ell,\psi_i)$ can be broken up into a convolution of the well-studied mass function with the conditional luminosity function:

$$P(L_{sh},\ell,\psi_i)d\ell \propto \ell^2 d\ell \int_{M_{\rm min}}^{M_{\rm max}} dM \frac{dN\,[r(\ell,\psi_i)]}{dM\,dV} P[L_{sh}\,|\,M, r(\ell,\psi_i)], \tag{3}$$

[1] http://www-glast.slac.stanford.edu/software/IS/.

with $r(\ell,\psi_i)=\sqrt{\ell^2+d_\odot^2-2\ell d_\odot\cos\psi_i}$ where $d_\odot=8.5\,\mathrm{kpc}$ is the Galactocentric distance of the Sun. The assumption that the dark matter halo extends out to $R_G=220$ kpc leads to $\ell_{\rm max}=d_\odot\left[\cos\psi_i+\sqrt{-\sin^2\psi_i+(R_G/d_\odot)^2}\right]$. The lower limit on the mass integral, $M_{\rm min}$, is determined by the cutoff scale of the subhalo mass function in the Milky Way halo. Supersymmetric models with WIMP dark matter candidates typically have a cutoff scale in the dark matter power spectrum in the range $M_{\rm min}\sim 10^{-6}-10^{0}M_\odot$ [28–35]; motivated by these models, for all results here we will adopt a value of $M_{\rm min}=0.01M_\odot$. We discuss the impact of varying $M_{\rm min}$ about this fiducial value below. The upper limit on the halo mass (which is not particularly relevant since the mass function falls off fairly steeply) is taken to be $10^{10}M_\odot$. With this information, Eq. 2 can now be written as

$$P_1(F;\psi_i)\propto\Theta(F_{\rm max}-F)\int_0^{\ell_{\rm max}}d\ell\,\ell^4\int_{M_{\rm min}}^{M_{\rm max}}dM\frac{dN[r(\ell,\psi_i)]}{dMdV}P[L_{sh}=4\pi\ell^2F\mid M,r(\ell,\psi_i)]. \tag{4}$$

To complete this calculation, we need the mass function and conditional luminosity function. In Lee et al. [24], it was assumed that there is a one-to-one mapping between subhalo luminosity and the mass of a subhalo, namely $L_{sh}\propto M_{sh}$. For our analysis we determine the $L_{sh}-M_{sh}$ relation using the properties of simulated subhalos in a ΛCDM cosmology [36]. The properties of subhalos, including those that will be relevant for us such as the spatial distribution and the assigned gamma-ray luminosity, reflect the underlying process of non-linear structure growth. The complex interplay between formation redshift, time of accretion to the parent halo, and orbital and tidal evolution sets the characteristics of the luminosity-mass relationship of subhalos, as well as the radial distribution (see [36]). As a result of this process, subhalos with similar mass and Galactocentric radius will have a spread in their gamma-ray luminosities.

We include this non-zero scatter by using the conditional luminosity distribution found in [36],

$$P(\ln L_{sh}\mid M,r)=\frac{1}{\sqrt{2\pi}}\frac{1}{\sigma}\exp\left[-\frac{[\ln L_{sh}-\langle\ln L_{sh}\rangle]^2}{2\sigma^2}\right]. \tag{5}$$

For a dark matter halo with a concentration of approximately $c\approx 10$ (model C_0 in [36]), the mean luminosity $\langle L_{sh}\rangle$, as well as the spread about the mean luminosity σ depend on subhalo mass and Galactocentric radius via

$$\langle\ln(L_{sh}/\mathrm{s}^{-1})\rangle=77.4+0.87\ln(M/10^5M_\odot)-0.23\ln(r/50\mathrm{kpc})+\ln\left(\frac{f_{\rm SUSY}}{10^{-28}\,\mathrm{cm}^3\,\mathrm{s}^{-1}\,\mathrm{GeV}^{-2}}\right) \tag{6}$$

$$\sigma=0.74-0.0030\ln(M/10^5M_\odot)-0.011\ln(r/50\mathrm{kpc}). \tag{7}$$

The quantity $f_{\rm SUSY}$ is the particle physics parameter[2] governing the emission rate,

$$f_{\rm SUSY}=N_\gamma\frac{\langle\sigma v\rangle}{m_\chi^2}. \tag{8}$$

Here the mass of the dark matter particle is m_χ, $\langle\sigma v\rangle$ is the thermally averaged annihilation cross section times the velocity, and N_γ is the number of photons above 1 GeV emitted in the annihilation of a single dark matter pair. A thermally averaged cross section of $\langle\sigma v\rangle=3\times10^{-26}$ cm^3 s^{-1} leads to the correct thermal abundance of dark matter today so that our fiducial value of $f_{\rm SUSY}=10^{-28}\,\mathrm{cm}^3\,\mathrm{s}^{-1}\,\mathrm{GeV}^{-2}$ is easily accommodated in supersymmetric models [14, 37].

Thus the mean luminosity in Eq. (6) differs from that of Lee et al. [24] in several ways: it scales with mass as $L_{sh}\propto M^{0.87}$, in agreement with simple analytic estimates [38], as well as numerical simulation results [21, 39]). Furthermore, the luminosity depends on the radial position of subhalos ($L_{sh}\propto r^{-0.23}$), and we also include a non-zero scatter (Eq. (7)) about the mean value of the luminosity, a scatter which depends on the mass and the Galactocentric radius of subhalos.

Numerical simulations predict a mass function of the form

$$dN(r)/dMdV=A\frac{(M/M_\odot)^{-\beta}}{\tilde{r}(1+\tilde{r})^2}, \tag{9}$$

[2] We use the $f_{\rm SUSY}$ to conform to the literature, but nothing in our analysis depends on supersymmetry; all that matters is the combination of cross section, mass, and N_γ folded into $f_{\rm SUSY}$.

with $\beta \approx 1.9$ [40]. Here the radial dependence is through $\tilde{r} = r/r_s$, where r_s is the scale radius of the Milky Way halo ($r_s \approx 21$kpc). We normalize the mass function by utilizing the numerical result that roughly 10% of the mass of the Galactic halo ($M_G = 1.2 \times 10^{12} M_\odot$) is in subhalos of mass greater than $\sim 10^7 M_\odot$. With this assumption, the normalization constant is $A \approx 1.2 \times 10^4 M_\odot^{-1}\mathrm{kpc}^{-3}$. Simulations also suggest that the halo distribution may be less cuspy near the center than the dark matter profile, and may depend on the mass of the subhalo [41]. This may have implications on the expected annihilation signal from substructure as the overall number of counts along a particular line of sight will be lower than expected (especially if most of the signal arrives from nearby objects). Nevertheless, given the current uncertainties of the level of this effect, we do not include a core in the distribution of subhalos in this study, but we emphasize that the issue of substructure depletion in the inner regions of the Galaxy must be addressed in detail in future numerical simulations.

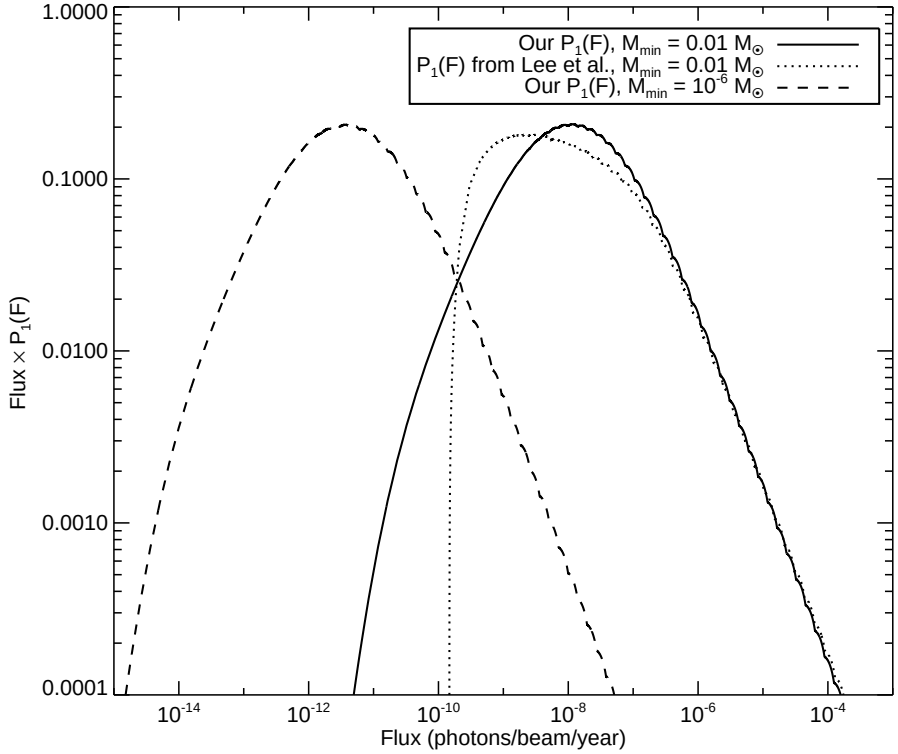

FIG. 1: Probability $P_1(F, \psi_i = 40^\circ)$ of observing flux F from a single halo in a given square degree pixel. We measure flux in units of photons/beam/year, where a 'beam' corresponds to the approximate effective area of the Fermi telescope, $A \sim 2000\mathrm{cm}^2$. The solid curve uses luminosity and mass functions from this paper with $M_{\rm min} = 0.01 M_\odot$, while the dashed curve uses the same functions with $M_{\rm min} = 10^{-6} M_\odot$. The dotted curve shows P_1 from Ref. [24] with $M_{\rm min} = 0.01 M_\odot$, re-scaled to have the same mean flux as our P_1 for the purpose of comparison.

With the above ingredients we construct the probability of observing a single subhalo with flux F in pixel i, $P_1(F, \psi_i)$, shown in Fig. 1 for $\psi_i = 40^\circ$. In generating this figure, we have used flux units of photons/beam/year, where the beam corresponds to the detector area of the Fermi telescope, $A \sim 2000\mathrm{cm}^2$ (the true effective area of Fermi is energy dependent so this value is only approximate). Of particular note in this figure is the smoother fall off at low flux in our model relative to the model of Lee et al. [24] (for the purpose of comparison we have scaled the Lee et al. [24] model so that it predicts the same mean flux as our model). As both of these models assume a sharp mass cut-off at the low end, the difference in fall-off at low flux follows directly from the scatter in luminosity for a given mass. When the low end mass cut-off, $M_{\rm min}$, is changed, we see from Fig. 1 that the mean flux per subhalo decreases but that the shape of $P_1(F)$ remains essentially unchanged.

Also, note that the PDF's for both models are very similar at the high flux end as a result of competing differences between the mass functions and the mass-luminosity relations of the two models. For a mass function that goes as $dN/dM \propto M^{-\beta}$ and a mass-luminosity relation such that $L_{sh} \propto M^\alpha$, it can be shown that for large values of F, $P_1(F) \propto F^\gamma$ with $\gamma = (1-\beta)/\alpha - 1$. For our model we have $\gamma = (1-1.9)/0.87 - 1 = -2.03$ while for the Lee et al. [24] model they have $\gamma = (1-2)/1 - 1 = -2$. Thus, in both models $P_1(F)$ is approximately proportional to F^{-2} for large F. Physically, our less-steep mass function means that we have more high mass (and thus high luminosity)

subhalos than the Lee et al. [24] model, but our less-steep luminosity function means that these subhalos are not as bright. The end result is that on the high flux end both models are very similar.

We use $P_1(F;\psi_i)$ to determine $P_{sh}(F;\psi_i)$, the probability of observing a total flux from multiple subhalos at angle ψ_i from the Galactic center. The two functions are related by

$$P_{sh}(F;\psi_i) = \mathcal{F}^{-1}\left\{e^{\mu(\psi_i)(\mathcal{F}\{P_1(F;\psi_i)\}-1)}\right\}, \tag{10}$$

where $\mathcal{F}$ indicates a Fourier transform with respect to F and μ is the mean number of subhalos in a given pixel:

$$\mu(\psi_i) = \Omega_{pixel}\int d\ell\ell^2 \int dM \frac{dN\left[r(\ell,\psi_i)\right]}{dMdV}. \tag{11}$$

Ω_{pixel} is the solid angle of a single pixel, taken here to be one square degree. Eq. 10 can be derived by assuming that the number of subhalos contributing to the photon counts in a single pixel is a Poisson random variable with mean μ and that each subhalo emits a flux F with probability $P_1(F;\psi_i)$. A detailed derivation of Eq. 10 is presented in the appendix of [24].

Finally, given $P_{sh}(F;\psi_i)$ we can construct $P(C_i)$, the probability of getting C counts in pixel i by applying Eq. (1). Fig. 2 shows the calculated $P(C_i)$ for the dark matter signal for one year of observation by the Fermi Telescope. Note that a Poisson distribution with the same mean number of counts has a significantly smaller probability of producing high-count pixels than the true $P(C_i)$. Also, note that despite the differences between our model and that of Lee et al. [24], both produce PDFs that are very similar. Apparently, the differences between the two models are washed out through the transition to $P_{sh}(F;\psi_i)$ and the subsequent discretization to produce $P(C_i)$. The similarity between the two models is encouraging: it suggests that the form of $P(C_i)$ is somewhat independent of the many assumptions that go into such models (e.g. the mass function, the luminosity function, $M_{\rm min}$, etc.), thus making our conclusions more robust.

In Table I we show the expected number of counts for our fiducial model, as well as four other models where we vary the cutoff scale of the mass function and the concentration (and substructure mass fraction) of the host Milky Way halo. The effect of the subhalo mass function cutoff on the photon counts is due to the fact that the luminosity increases with mass at a slower rate than the rate at which the abundance is increasing with mass - *numerous* small (and faint) subhalos yield a higher flux than *few* large and bright subhalos. The effect is not very large, as decreasing $M_{\rm min}$ by four orders of magnitude results in only a factor of ~ 4.5 increase in the photon counts. Still, understanding the low-mass cutoff scale of the subhalo mass function is important in any future interpretation of γ-ray data.

The high and low concentration models in Table I refer to models C_+ and C_- respectively in [36]. They represent host Milky Way halos with high ($c \geq 13$) and low ($c \leq 7$) concentrations. The luminosity PDF is a weak function of concentration, except perhaps in the very inner regions of the halo. The normalization of the subhalo mass function, however, depends somewhat strongly on the host concentration. High concentration host halos have a lower normalization of substructure $f \approx 0.08$ (where f is the mass fraction of subhalos relative to the total halo mass) relative to low concentration halos which have a higher normalization of substructure $f \approx 0.3$. This is an outcome of hierarchical structure formation. High concentration host halos were formed earlier and therefore their constituent subhalos evolved for a longer period of time in the presence of the tidal field of the host, thus the subhalo survival rate is lower than in the low concentration (recently formed) hosts. As can be seen from Table I, varying the host concentration changes the total photon counts by at most about 60%.

Model	Mean Counts at $\psi = 40^\circ$	Approximate Total Counts
Fiducial	0.83	6600
Fiducial with $M_{\rm min} = 10^{-6} M_\odot$	1.36	29800
Fiducial with $M_{\rm min} = 10^{2} M_\odot$	0.49	4000
High Host Concentration	1.57	12100
Low Host Concentration	0.91	7300

TABLE I: The mean number of signal counts in one year per square degree at an angle $\psi = 40^\circ$ relative to the Galactic center, and the approximate total signal counts on the sky at latitudes greater than $b > 40^\circ$ for our fiducial model and two models which demonstrate the effects of our lack of knowledge of the subhalo mass function cutoff scale. The low and high concentration models represent extreme models of the host Milky Way properties.

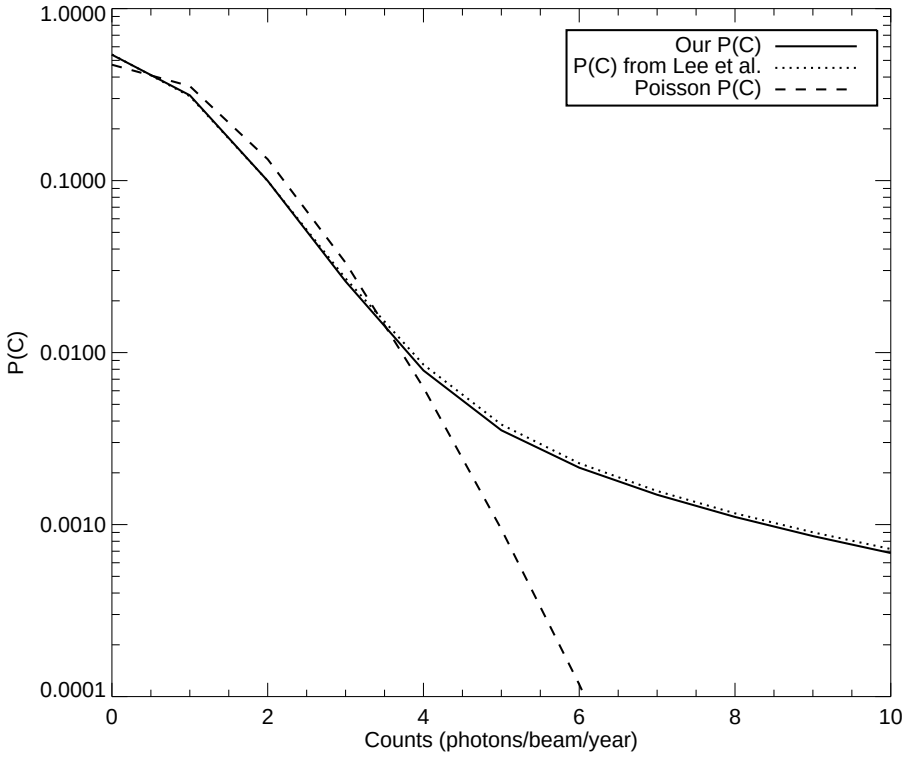

FIG. 2: $P_{sh}(C, \psi_i)$, the probability of observing C counts in pixel i from all subhalos along the line of sight where here $\psi_i = 40^\circ$. The $P_{sh}(C, \psi_i)$ predicted by our model is compared with that of Lee et al. [24], which we have scaled to have the same mean as our model. The two functions are very similar despite the underlying differences of the two models. Both differ significantly from a pure Poisson distribution with the same mean number of counts.

B. The Backgrounds: Galactic and Extra-Galactic

We now move on to discuss the sources of gamma-rays that we consider in our analysis in addition to the signal from subhalos. For ease of book-keeping, we will simply describe gamma-rays from non-subhalo sources as either Galactic or Extra-Galactic in origin, and now discuss each of these components in turn.

Galactic Background– Cosmic ray interactions with atomic (HI) and molecular (primarily H_2 and CO) gas are the source of diffuse Galactic gamma-ray emission. The emission results from the decay of neutral pions produced in hadronic collisions as well as inverse Compton scattering of the interstellar radiation field by electrons, and to a lesser extent bremsstrahlung emission from the interstellar medium. Accurately modeling this emission is challenging [42] and indeed crucial for the interpretation and extraction of a dark matter component in the gamma-ray background.

In our analysis we utilize the standard diffuse gamma-ray emission model of the LAT science team [3]. We take the LAT team model, which is based on the observed distribution of gas as well as known point sources, as the prediction of the number of counts in the i^{th} pixel, $C_i^{\rm b,Fermi}$, for one year of observation. Note that the predicted number of counts generated by the signal depends only on the angle ψ_i that separates the pixel from the center of the Galaxy. However the backgrounds are different: $C_i^{\rm b,Fermi}$ depends on both l_i and b_i, and hence not only on ψ_i but also on the azimuthal position in the annulus.

In each angular pixel, our total number of counts is obtained by summing over all photons with energy above 1 GeV. We choose this energy threshold mainly because most of the photons emitted by dark matter pairs with mass ~ 100 GeV or greater are above this energy, and also because the diffuse Galactic emission is observed to be a steeply falling power law near these energies. A different choice of energy threshold is trivial to incorporate into the dark matter model since it simply corresponds to different N_γ in the definition of $f_{\rm SUSY}$, so changing the energy threshold

[3] http://fermi.gsfc.nasa.gov/ssc/data/access/lat/BackgroundModels.html

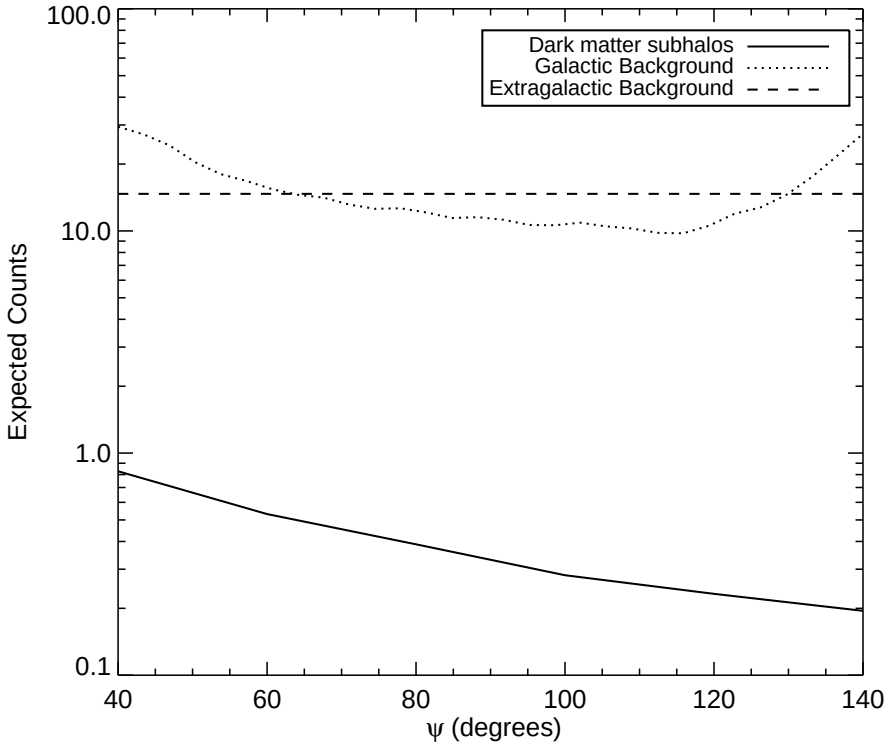

FIG. 3: Expected counts per one square degree pixel above 1 GeV in 1 year of Fermi data from dark matter annihilation in subhalos when $f_{\rm SUSY} = 10^{-28}$ cm^3 s^{-1} GeV^{-2}, the Galactic background, and the diffuse extra-Galactic background. The counts are given in a one square degree pixel.

corresponds to changing $f_{\rm SUSY}$.

Using the LAT team diffuse model, we simulate sky maps of diffuse gamma-ray emission. When fitting these maps to our model, we introduce one free parameter, given by the amplitude of the counts b_g. So when considering the diffuse Galactic emission, our model is simply given by

$$C_i^{\rm gal} = b_g C_i^{\rm gal,Fermi} \tag{12}$$

with the true value of $b_g = 1$.

Fig. 3 shows the counts from the diffuse Galactic model in a one square degree pixel as a function of angle from the Galactic center, ψ, with our fiducial normalization ($b_g = 1$). Also plotted is the expected signal flux from dark matter subhalos in equally sized pixels. For all angles the counts from the Galactic model are at least an order of magnitude greater than the counts from subhalos. As expected, the signal flux falls off with increasing ψ because the number density of subhalos decreases with distance from the galactic center (see Eq. 9). The galactic background increases towards $\psi = 0^\circ$ and $\psi = 180^\circ$ because most of the diffuse emission is from the galactic plane.

Extra-Galactic Background– The isotropic component of the LAT team diffuse model is a result of the emission from extra-Galactic and instrumental sources. Over the energy range of ~ 100 MeV - 100 GeV, and for $b > 40^\circ$, the isotropic component ascribed to extragalactic emission is well fit by a power law with index 2.41 [43]. The updated diffuse model indicates that above 1 GeV, the normalization of the extra-Galactic component is comparable to that of the dominant component of Galactic emission that arises from neutral π decay. In our analysis, we will simply model the extra-Galactic component by a number of counts with an amplitude that is allowed to be free,

$$C_i^{\rm eg} = b_{eg} C_i^{\rm eg,Fermi}. \tag{13}$$

Fig. 3 shows our fiducial normalization ($b_{eg} = 1$) is one in which the extra-Galactic flux is about 30 times greater than the subhalo flux, contributing ~ 15 counts above a GeV in one square degree pixel.

III. SIMULATED MAPS

Armed with the probability distribution in Eq. (1), we can generate simulated maps of the sky for a given experiment specified by its exposure, E_i. First, though, we construct a simpler map, shown in Fig. 4 to assess "by eye" the impact of the assumed subhalo PDF. Both maps in Fig. 4 are simulations which include the subhalo dark matter signal only. The central 40° is not used so it is zeroed out in all of our maps, since it will be dominated by Galactic emission. The top panel map in Fig. 4 is drawn from a model with the same number of expected counts in every pixel as the model introduced in §II. The counts in each pixel in this map, however, are drawn from a Poisson distribution. The bottom panel has photons drawn from the "true" dark matter PDF. Fig. 2 showed how different the subhalo PDF is from Poisson, and Fig. 4 illuminates this difference very graphically. There are a number of pixels with many counts (of order ten) in marked contrast to the Poisson map which has no high-count pixels.

This visual impression is hidden in a map with backgrounds. Fig. 5 shows two maps with the same dark matter counts as in Fig. 4, but with counts from the backgrounds added in. It is no longer possible to tell the distributions apart by eye, so a more careful statistical probe is needed. We analyze the maps in the next section to see if the subhalo signal can be extracted.

IV. ANALYSIS

We will analyze the simulated sky constructed in the previous section in two different ways. First, we will carry out a simple Poisson analysis to obtain constraints on the parameters. That is, we fit the data by maximizing a likelihood which assumes (incorrectly) that all sources of photons are generated from a Poisson distribution,

$$\mathcal{L}^{\rm Poisson}(f_{\rm SUSY}, b_g, b_{eg}) = \prod_{i=1}^{N_p} \mathcal{P}\left[E_i \bar{F}_i(f_{\rm SUSY}) + C_i^{\rm g}(b_g) + C_i^{\rm eg}(b_{eg}); C_i\right]. \tag{14}$$

In Eq. 14, the parameters specifying the amplitudes of the background are b_g and b_{eg}; C_i is the observed number of counts in pixel i (there are a total of N_p pixels); $\bar{F}_i$ is the mean expected flux from dark matter annihilations in pixel i; and $\mathcal{P}[A;B]$ again is the Poisson probability of observing B counts in a pixel in which the mean expected number of counts is A. We emphasize that we are (purposely) doing things wrong here: we are analyzing a map generated from one distribution assuming incorrectly that the map is Poisson. One of the goals is to determine whether this flawed (yet simpler) analysis obtains the correct answer. We fit the data to the three free parameters, find the best fit value in this 3D space, and then identify 1-, 2-, and 3-sigma constraints by finding regions within which $\int df_{\rm SUSY} db_g db_{eg} = 0.68, 0.95, 0.997$. The best fit value is termed an estimator, the Poisson estimator.

A second way to analyze these simulated maps is to use the "true" likelihood. We want to see how much better this approach is than the Poisson analysis. Here we use the exact likelihood,

$$\mathcal{L} = \prod_{i=1}^{N_p} P(C_i | f_{\rm SUSY}, b_g, b_{eg}), \tag{15}$$

where $P(C_i|f_{\rm SUSY}, b_g, b_{eg})$ is given in Eq. (1). Again, we can form an estimator and allowed regions for the parameters; we call this estimator the "true" or "exact" estimator.

We will apply each of these estimators to the signal+background maps constructed in § III, but first let us work on the background-free maps. There it was easy to tell the difference between the 2 PDF's by eye, so we expect to see considerable differences in the analyses. Fig. 6 show the results of ten runs applying each estimator. The "true" likelihood extracts the correct value accurately and obtains small error bars. In contrast, the Poisson likelihood consistently mis-estimates the value of $f_{\rm SUSY}$. Apparently, the Poisson estimator is misled by the many pixels with few counts so systematically shifts the mean number of counts lower, thereby leading to an under-estimate of $f_{\rm SUSY}$.

When backgrounds are added in, it becomes less important to use the correct PDF. To see this, consider the constraints obtained on one simulated map using the two estimators, as shown in Fig. 7. In this realization, both estimators recapture the true parameter values. The errors on the parameters are larger when the simpler, Poisson estimator is used, but the overall impression is that using the Poisson estimator would not do appreciable damage.

To test this further, we generated 10 such maps. Fig. 8 shows the distribution of best fit values of $f_{\rm SUSY}$, b_{eg}, and b_g from these runs. The means are both close to the true values of the parameters. The errors from the Poisson analysis are larger by 50 percent, so knowing the PDF does help, but the danger of a bias appears to be eliminated.

For observation times greater than the one year that we assume in our analysis, the size of the error contours will of course decrease. Since $f_{\rm SUSY}$ is proportional to the photon flux and since we have shown that the errors in $f_{\rm SUSY}$

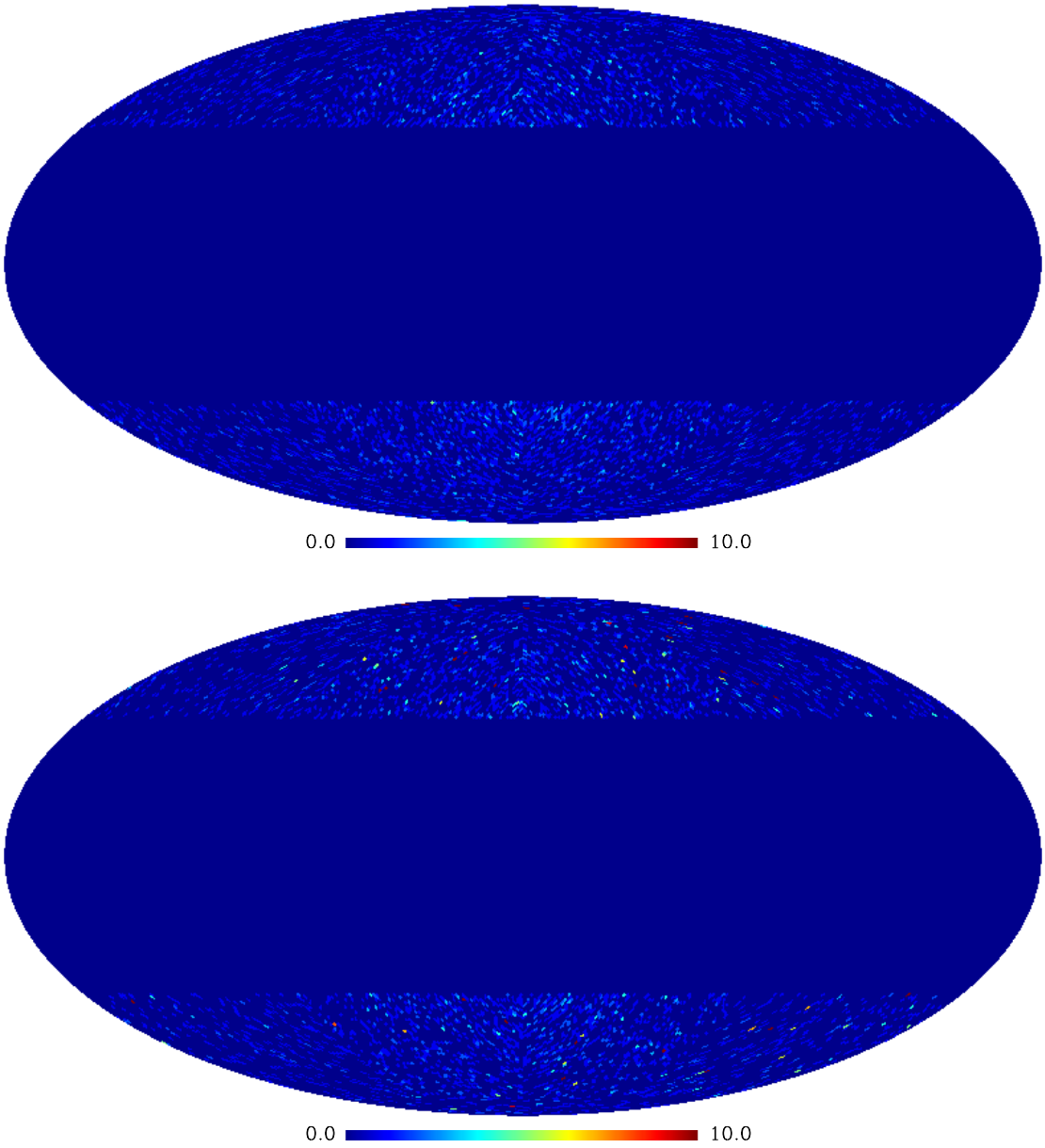

FIG. 4: Simulated maps of the photons above one GeV in Fermi produced by the annihilations of dark matter in subhalos. *Top panel:* Simulated counts drawn from a Poisson distribution with the same number of expected events as the dark matter PDF. *Bottom panel:* Photons drawn from the dark matter PDF.

are reasonably described by Poisson statistics, the fractional error in our determination of $f_{\rm SUSY}$ will scale in inverse proportion to the square root of the exposure time. Therefore, with data covering the five year expected lifetime of the Fermi Telescope, we expect the error contours on $f_{\rm SUSY}$ to be about 55% smaller than shown here.

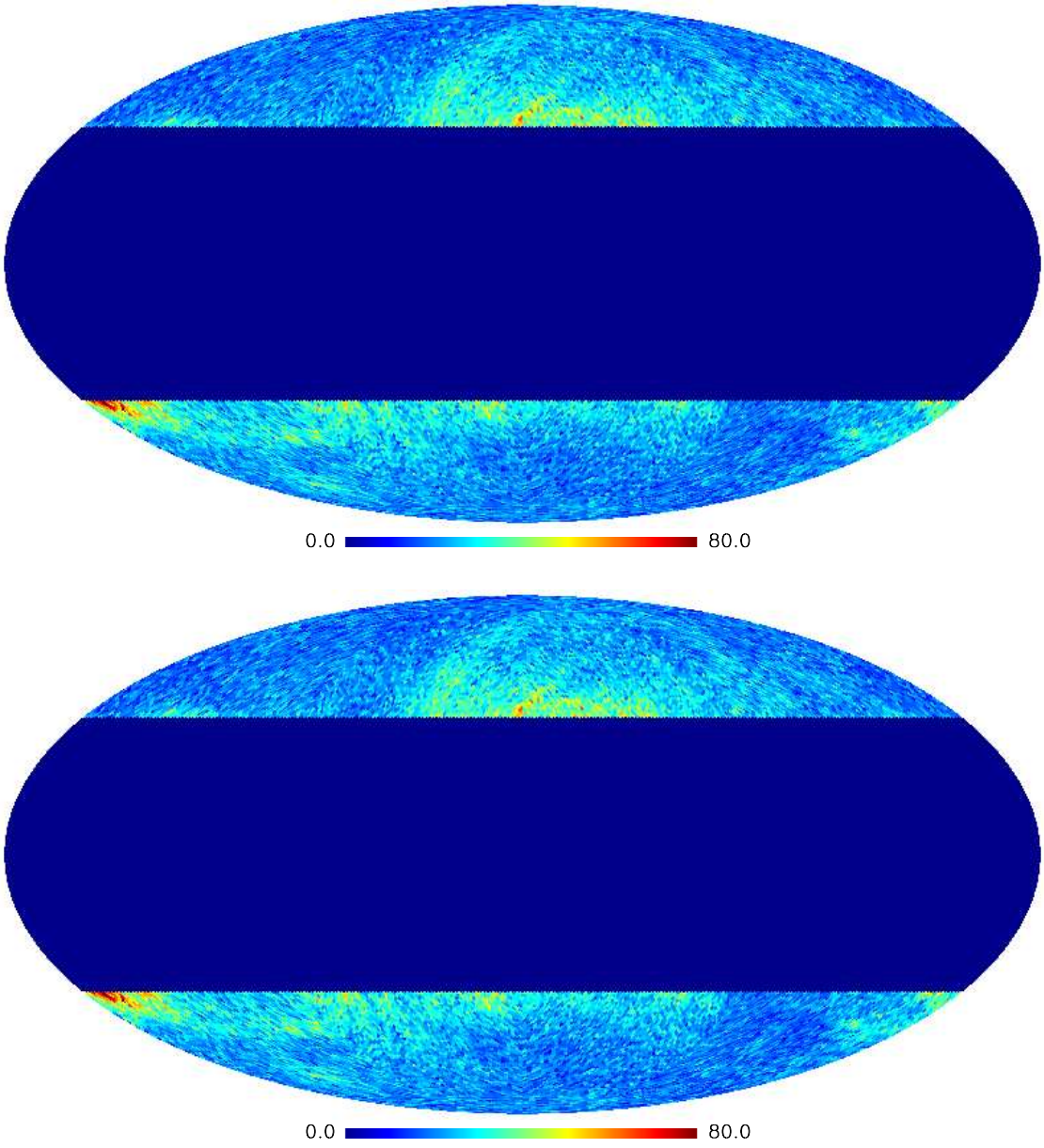

FIG. 5: Same as Fig. 4 but with the addition of backgrounds from the Galaxy and unresolved extra-Galactic sources.

V. CONCLUSIONS

The gamma ray signal from annihilation of Galactic dark matter subhalos has a probability distribution function which is very different from a Poisson distribution with the same number of mean counts. This feature, initially explored in Ref. [24] and fleshed out here with a slightly less restrictive model, should produce in Fermi many pixels with zero or small number of counts but a finite set with large number of counts. We have addressed here the question of how this PDF will affect future analyses and concluded that, once the backgrounds are added in, a simple analysis which assumes a Poisson PDF is unbiased and only slightly less powerful than one which uses the full, correct PDF.

To some extent this is good news: there is a tension between analyses which are agnostic as to the nature of the signal and those which assume that many of its underlying features are known and are simply fitting for parameters.

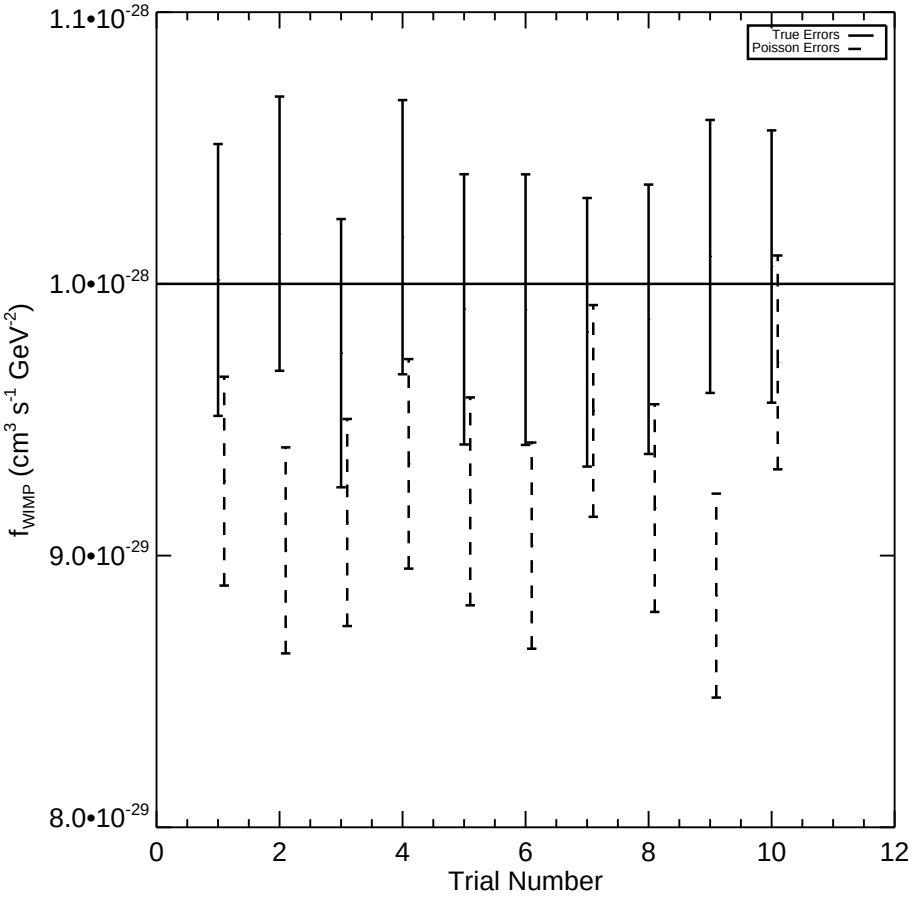

FIG. 6: Best fit values of $f_{\rm SUSY}$ from multiple runs when backgrounds are not included. The true likelihood recaptures the input value of $f_{\rm SUSY} = 10^{-28}\,{\rm cm}^3\,{\rm s}^{-1}\,{\rm GeV}^{-2}$, while the Poisson likelihood systematically under-estimates $f_{\rm SUSY}$. The error bars shown represent 3σ confidence intervals.

Those in the first class are more robust and believable because they are based are fewer assumptions; those in the second are more powerful statistically and will lead to tighter constraints on the properties of dark matter. When we find little loss in statistical power from dropping an assumption and moving towards more agnostic estimators, we should become more optimistic about our chances of extracting a signal hidden in backgrounds. This is perhaps the most important result of this work.

Lingering in our discussion, and in the literature at large (see, e.g., [9]), is the question how much information will the data contain? The answer to this is encoded in the likelihood function, and our conclusions are that one year of Fermi data contains enough information to detect a value of $f_{\rm SUSY} = 10^{-28}$ cm^3 s^{-1} GeV^{-2}. We are not claiming that a robust detection of this small a signal can be expected (for an incomplete sample of analyses, see [43–46]), but just that the information is there and we should attempt to extract it.

Our analysis has included/assumed two types of information about the signal and backgrounds: the angular distribution and the PDF. We have not included two other potential discriminants: the spectral shapes of the different components and the angular two-point functions. The former is easy to include within the formalism developed here, and we plan to address this in future work. The latter has been explored by a number of authors [26, 47–51] in the form of the C_l's. There is a connection between our work and the fluctuations explored elsewhere: we have implicitly assumed a flat C_l spectrum, but one that has a larger amplitude than Poisson (because the PDF is not Poisson). Whether or not this set of assumptions includes all of the effects explored elsewhere is an open question.

Acknowledgments– This work has been supported by the National Science Foundation Grant AST-0908072 and by the US Department of Energy, including grant DE-FG02-95ER40896. Support for LS for this work was provided

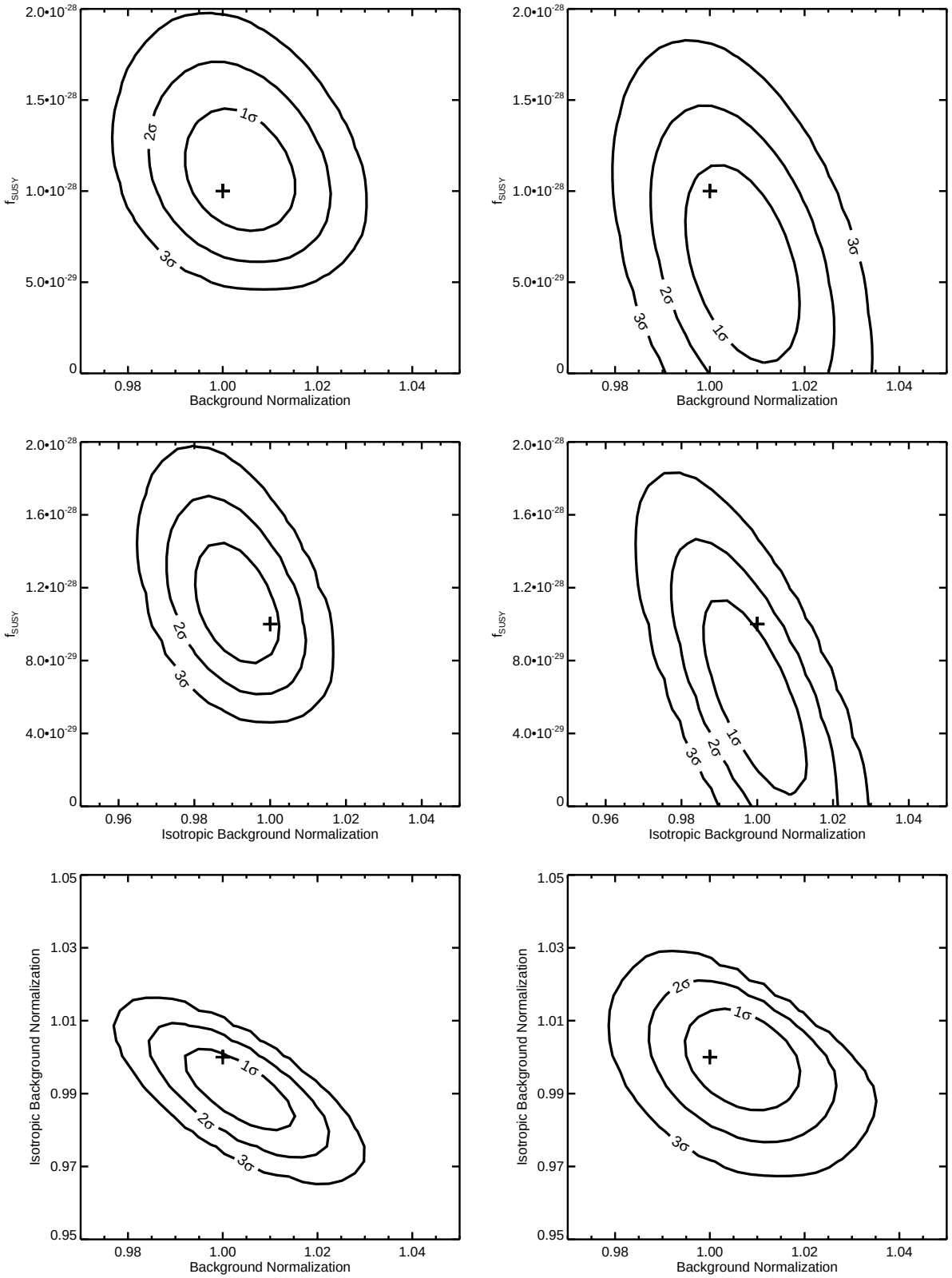

FIG. 7: Constraints from one simulated map of signal and backgrounds on the 3 parameters when the underlying model has $f_{\rm SUSY} = 10^{-28}\,{\rm cm}^3\,{\rm s}^{-1}\,{\rm GeV}^{-2}$ and $b_g = b_{eg} = 1$. *Left panels:* Results using the "true" PDF for dark matter. *Right panels:* Constraints assuming a Poisson likelihood. The Poisson analysis retrieves the correct result even though it assumes the wrong PDF; the allowed region is slightly larger if the true likelihood is not known, but there is no bias.

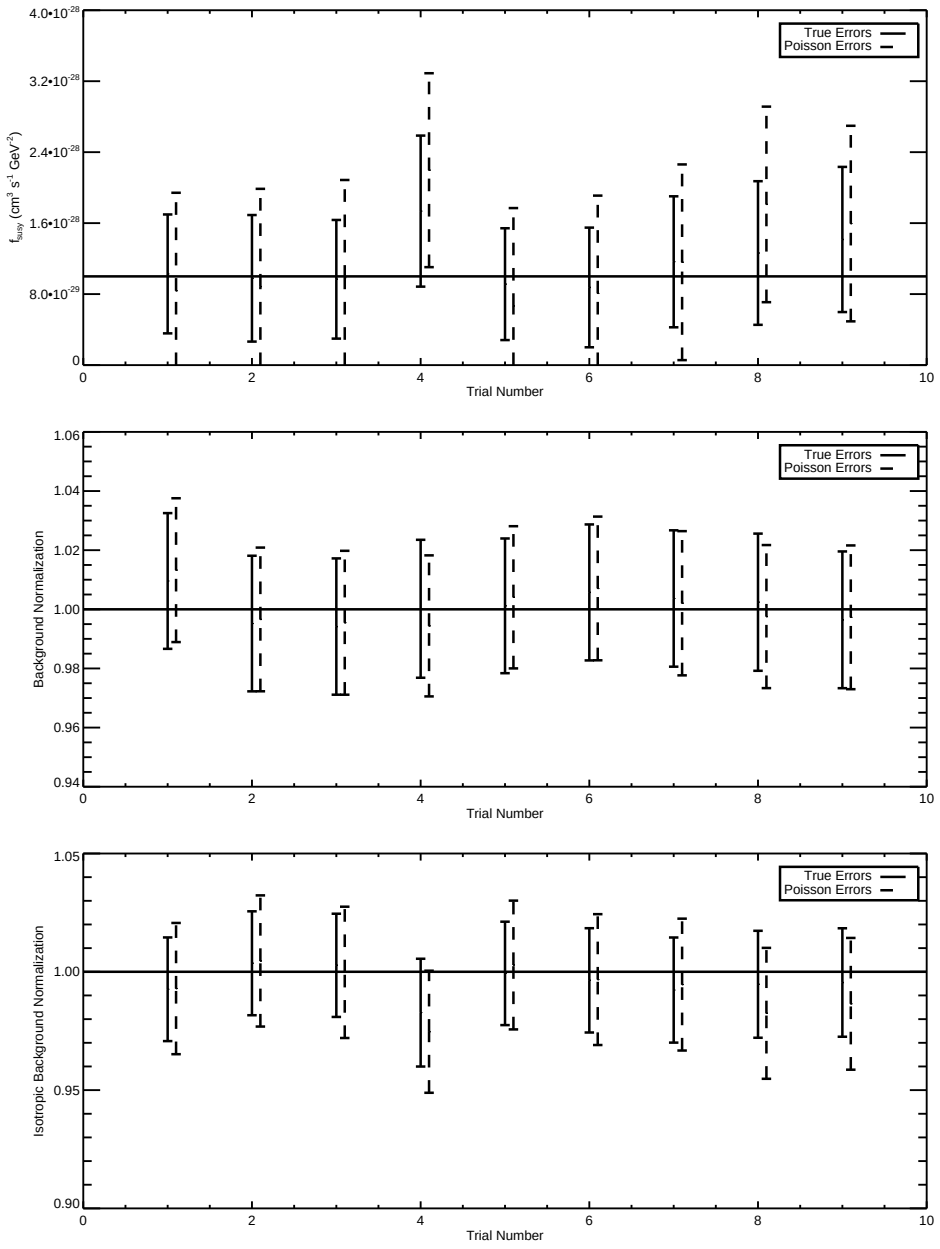

FIG. 8: Best fit values of $f_{\rm SUSY}$ and background amplitudes from multiple runs. The true values ($f_{\rm SUSY} = 10^{-28}$ cm^3 s^{-1} GeV^{-2}, $b_g = 1, b_{eg} = 1$) are recaptured by both estimators, but the errors – especially on $f_{\rm SUSY}$ – are about 50 percent larger when the Poisson estimator is used. The error bars shown represent 3σ confidence intervals.

by NASA through Hubble Fellowship grant HF-51248.01-A awarded by the Space Telescope Science Institute, which is operated by the Association of Universities for Research in Astronomy, Inc., for NASA, under contract NAS 5-26555.

[1] G. Bertone, D. Hooper, and J. Silk, Phys. Rept. **405**, 279 (2005), hep-ph/0404175.
[2] A. Birkedal, K. Matchev, and M. Perelstein, Phys. Rev. D **70**, 077701 (2004), arXiv:hep-ph/0403004.
[3] J. L. Feng, S. Su, and F. Takayama, Physical Review Letters **96**, 151802 (2006), arXiv:hep-ph/0503117.
[4] A. Drukier and L. Stodolsky, Phys. Rev. D **30**, 2295 (1984).
[5] M. W. Goodman and E. Witten, Phys. Rev. D **31**, 3059 (1985).
[6] J. Silk and M. Srednicki, Physical Review Letters **53**, 624 (1984).

[7] J. E. Gunn, B. W. Lee, I. Lerche, D. N. Schramm, and G. Steigman, Astrophys. J. **223**, 1015 (1978).
[8] Y. A. Golubkov, R. V. Konoplich, R. Mignani, D. Fargion, and M. Y. Khlopov, Soviet Journal of Experimental and Theoretical Physics Letters **69**, 434 (1999), arXiv:astro-ph/9903086.
[9] E. A. Baltz et al., JCAP **0807**, 013 (2008), 0806.2911.
[10] C. M. Hui and f. t. V. Collaboration, AIP Conf. Proc. **1085**, 407 (2009), 0810.1913.
[11] O. Adriani et al. (PAMELA), Nature **458**, 607 (2009), 0810.4995.
[12] E. Resconi and f. t. I. Collaboration, Nucl. Instrum. Meth. **A602**, 7 (2009), 0807.3891.
[13] L. Bergstrom, P. Ullio, and J. H. Buckley, Astropart. Phys. **9**, 137 (1998), astro-ph/9712318.
[14] N. Fornengo, L. Pieri, and S. Scopel, Phys. Rev. **D70**, 103529 (2004), hep-ph/0407342.
[15] E. A. Baltz, J. E. Taylor, and L. L. Wai, Astrophys. J. Lett. **659**, L125 (2007), astro-ph/0610731.
[16] T. M. Venters and V. Pavlidou, AIP Conf. Proc. **921**, 163 (2007), 0704.2417.
[17] D. Hooper and P. D. Serpico, JCAP **0706**, 013 (2007), astro-ph/0702328.
[18] A. Cuoco, J. Brandbyge, S. Hannestad, T. Haugbølle, and G. Miele, Phys. Rev. D **77**, 123518 (2008), 0710.4136.
[19] S. Dodelson, D. Hooper, and P. D. Serpico, Phys. Rev. **D77**, 063512 (2008), 0711.4621.
[20] M. Kuhlen, J. Diemand, and P. Madau, AIP Conf. Proc. **921**, 135 (2007), 0704.0944.
[21] M. Kuhlen, J. Diemand, and P. Madau (2008), 0805.4416.
[22] F. W. Stecker and M. H. Salamon (2001), astro-ph/0104368.
[23] C. D. Dermer, AIP Conf. Proc. **921**, 122 (2007), 0704.2888.
[24] S. K. Lee, S. Ando, and M. Kamionkowski (2008), 0810.1284.
[25] S. Dodelson, A. V. Belikov, D. Hooper, and P. Serpico, Phys. Rev. **D80**, 083504 (2009), 0903.2829.
[26] J. M. Siegal-Gaskins and V. Pavlidou (2009), 0901.3776.
[27] V. Springel et al., Nature **456N7218**, 73 (2008).
[28] S. Hofmann, D. J. Schwarz, and H. Stöcker, Phys. Rev. D **64**, 083507 (2001), arXiv:astro-ph/0104173.
[29] X. Chen, M. Kamionkowski, and X. Zhang, Phys. Rev. **D64**, 021302 (2001).
[30] S. Profumo, K. Sigurdson, and M. Kamionkowski, Phys. Rev. Lett. **97**, 031301 (2006), astro-ph/0603373.
[31] C. Schmid, D. J. Schwarz, and P. Widerin, Phys. Rev. D **59**, 043517 (1999), arXiv:astro-ph/9807257.
[32] A. M. Green, S. Hofmann, and D. J. Schwarz, Mon. Not. Roy. Astron. Soc. **353**, L23 (2004), astro-ph/0309621.
[33] A. M. Green et al., JCAP **0508**, 003 (2005), astro-ph/0503387.
[34] A. Loeb and M. Zaldarriaga, Phys. Rev. **D71**, 103520 (2005), astro-ph/0504112.
[35] G. D. Martinez, J. S. Bullock, M. Kaplinghat, L. E. Strigari, and R. Trotta, JCAP **0906**, 014 (2009), 0902.4715.
[36] S. M. Koushiappas, A. R. Zentner, and A. V. Kravtsov, ArXiv e-prints (2010), 1006.2391.
[37] L. Bergstrom, J. Edsjo, and P. Ullio, Phys. Rev. Lett. **87**, 251301 (2001), astro-ph/0105048.
[38] L. E. Strigari, S. M. Koushiappas, J. S. Bullock, and M. Kaplinghat, Phys. Rev. **D75**, 083526 (2007), astro-ph/0611925.
[39] J. Diemand, M. Kuhlen, and P. Madau, Astrophys. J. **657**, 262 (2007), astro-ph/0611370.
[40] V. Springel et al., Mon. Not. Roy. Astron. Soc. **391**, 1685 (2008), 0809.0898.
[41] E. D'Onghia, V. Springel, L. Hernquist, and D. Keres, Astrophys. J. **709**, 1138 (2010), 0907.3482.
[42] A. A. Abdo et al. (Fermi LAT), Phys. Rev. Lett. **103**, 251101 (2009), 0912.0973.
[43] A. A. Abdo et al. (Fermi-LAT) (2010), 1002.4415.
[44] M. Cirelli, P. Panci, and P. D. Serpico (2009), 0912.0663.
[45] K. N. Abazajian, P. Agrawal, Z. Chacko, and C. Kilic (2010), 1002.3820.
[46] G. Hütsi, A. Hektor, and M. Raidal, Journal of Cosmology and Astro-Particle Physics **7**, 8 (2010), 1004.2036.
[47] S. Ando and E. Komatsu, Phys. Rev. **D73**, 023521 (2006), astro-ph/0512217.
[48] S. Ando, E. Komatsu, T. Narumoto, and T. Totani, Mon. Not. Roy. Astron. Soc. **376**, 1635 (2007), astro-ph/0610155.
[49] S. Ando, E. Komatsu, T. Narumoto, and T. Totani, Phys. Rev. **D75**, 063519 (2007), astro-ph/0612467.
[50] J. M. Siegal-Gaskins, JCAP **0810**, 040 (2008), 0807.1328.
[51] B. S. Hensley, J. M. Siegal-Gaskins, and V. Pavlidou (2009), 0912.1854.